Supplementary dating performed at Xi'an Jiaotong University.

Additional ^{230}Th dating of two samples was performed at the Isotope Laboratory, Xi'an Jiaotong University using multi-collector inductively coupled plasma mass spectrometers (MC-ICP-MS) (Thermo-Finnigan Neptune-*plus*). We used standard chemistry procedures to separate U and Th for dating (Edwards et al., 1987). A triple-spike (^{229}Th–^{233}U–^{236}U) isotope dilution method was employed to correct for instrumental fractionation and determine U-Th isotopic ratios and concentrations. The instrumentation, standardization and half-lives are reported in Cheng et al. (2000) and (2013). All U-Th isotopes were measured on a MasCom multiplier behind the retarding potential quadrupole in the peak-jumping mode. We followed similar procedures of characterizing the multiplier as described in Cheng et al. (2000). Uncertainties in U-Th isotopic data were calculated offline at 2σ level, including corrections for blanks, multiplier dark noise, abundance sensitivity, and contents of the same nuclides in spike solution. Corrected ^{230}Th ages assume the initial ^{230}Th/^{232}Th atomic ratio of 4.4 ±2.2 x10^{-6}, the values for a material at secular equilibrium with the bulk earth ^{232}Th/^{238}U value of 3.8.

Cheng, H., Edwards, R. L., Hoff, J., Gallup, C. D., Richards, D. A., Asmerom, Y. 2000. The half-lives of U-234 and Th-230. *Chem. Geol*. **169**, 17–33.

Cheng, H., Edwards, R. L., Shen, C.–C., Polyak, V. J., Asmerom, Y., Woodhead, J., Hellstrom, J., Wang, Y., Kong, X., Spötl, C., Wang, X., Calvin Alexander, E. 2013. Improvements in ^{230}Th dating, ^{230}Th and ^{234}U half-life values, and U–Th isotopic measurements by multi-collector inductively coupled plasma mass spectrometry. *Earth Planet. Sci. Lett.* **371**, 82–91.

Edwards, R. L., Chen, J. H., Wasserburg, G. J. 1987. ^{238}U, ^{234}U, ^{230}Th, ^{232}Th systematics and the precise measurement of time over the past 500,000 years. *Earth Planet. Sci. Lett*. **81**, 175–192.

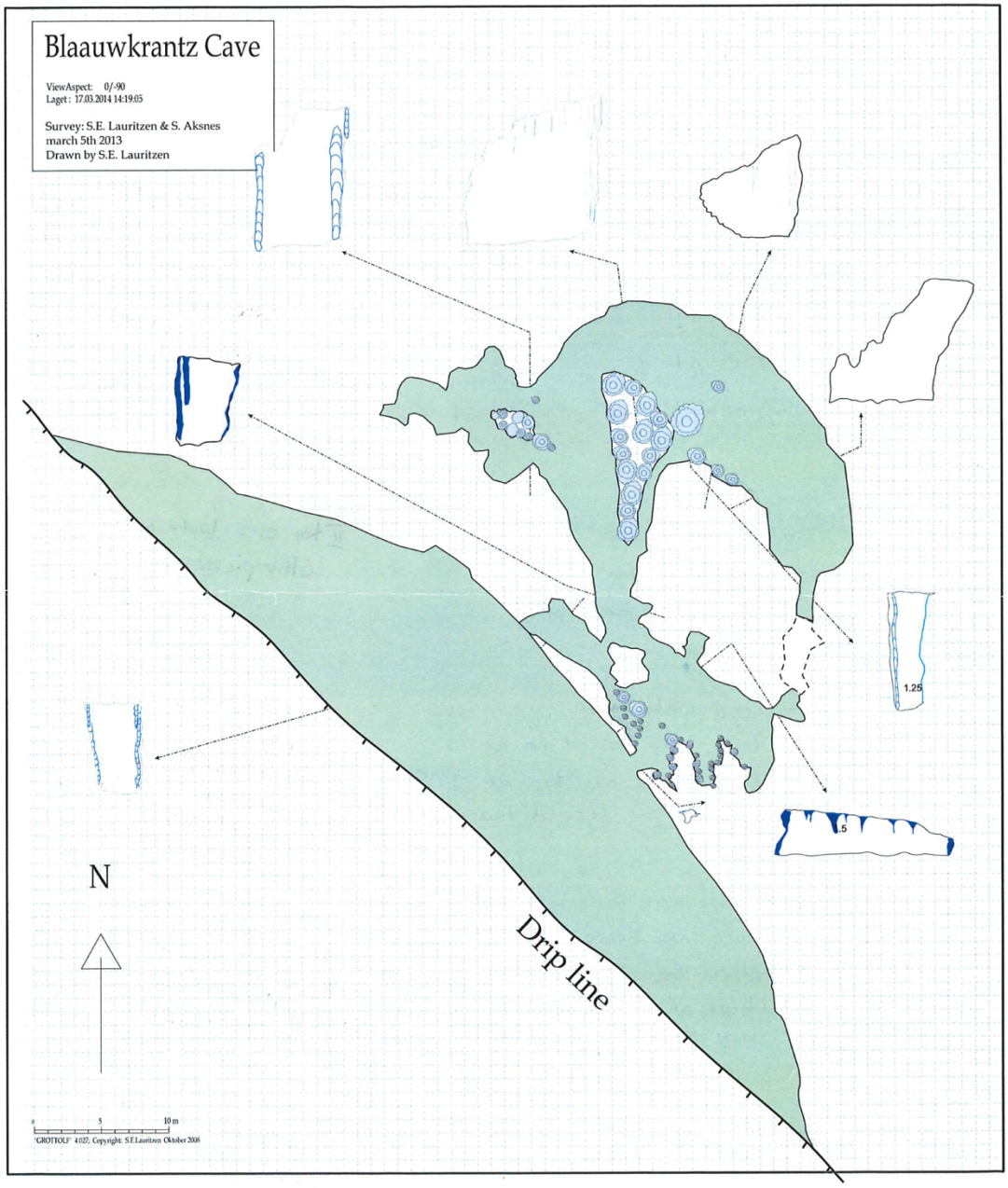

Figure S1: Blauwkrantz cave map. A 3D reconstruction of the cave performed by Ole Fredrik Unhammer can be found at : https://sketchfab.com/3d-models/bloukrans-cave-south-africa-600e7347a07a4b26a39bc4eefd5526e2 (Unhammer, O. F., Lauritzen, S.-E., Henshilwood, C. *Photogrammetric mapping of complex cave chambers at Bloukrans Cave, South Africa: Structural, Morphological and Speleogenetic Information*. 26th International Karstological School "Classical Karst" SHOW CAVES AND SCIENCE; 2018-06-18 - 2018-06-22)

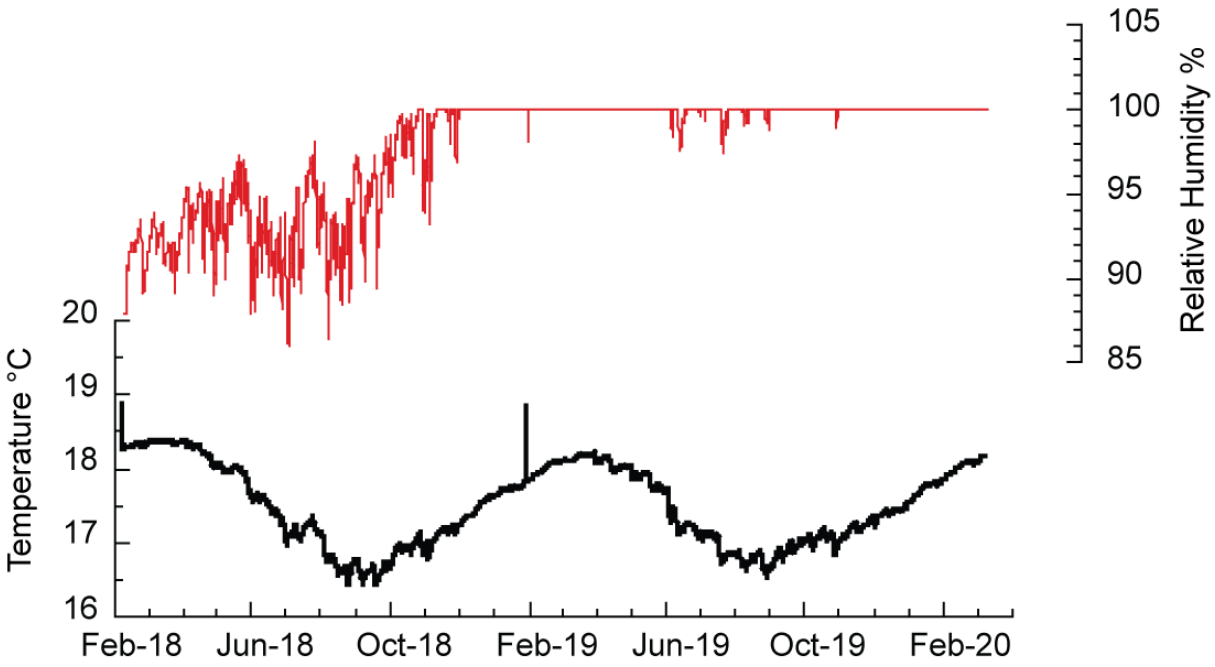

Figure S2: HOBO logger data recorded from February 2018 to Mars 2020. Top: relative humidity (red); bottom: cave temperature (black).
The cave was not dripping in February 2018 when the logger was first installed and recorded relative humidity ~90-95%. Dripping was active in January 2019 and March 2020 when relative humidity of 100% were recorded.

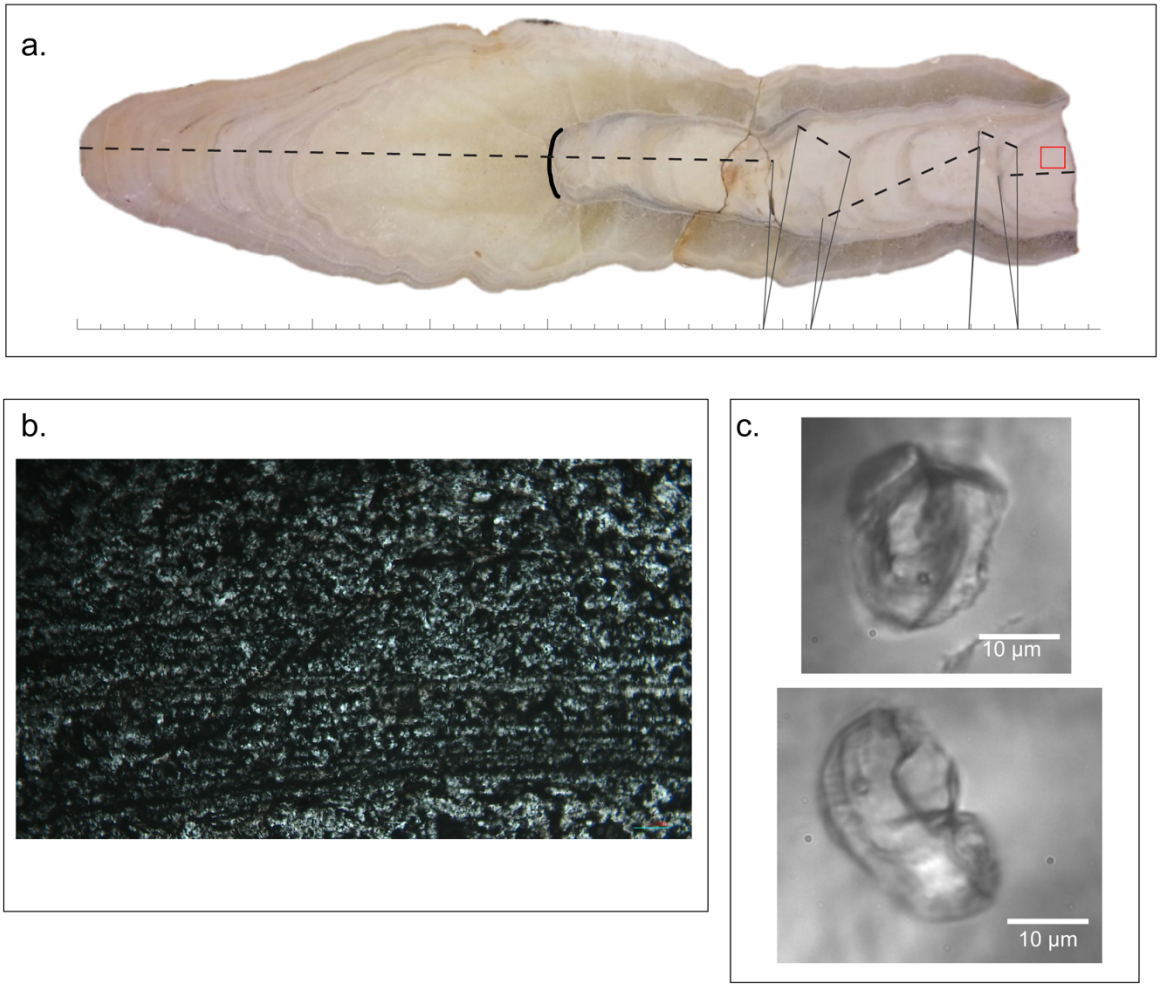

Figure S3: a. Speleothem BL3 from Bloukrantz cave. A hiatus (black line) is visible at mid-length with a change in fabric/color. The red rectangle indicates the approximate location of the thin section shown in b; b. Thin section of the microcrystalline fabric with a dark layer clearly visible in the lower part; c. Examples of nucleated bubbles of analyzed fluid inclusions.

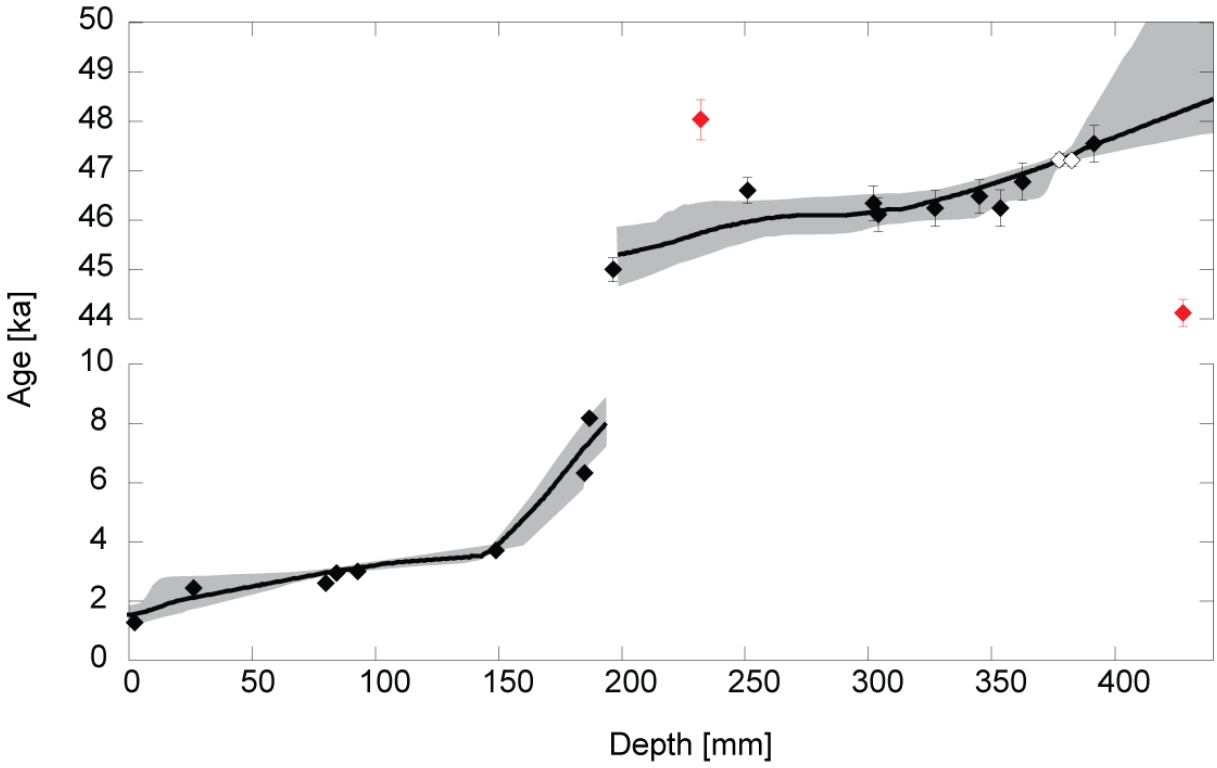

Figure S4: Age model for BL3 using StalAge (Scholz and Hoffmann 2011) and performed as two distinct sections. Grey shading corresponds to 95% confidence interval of the age model. Error bars are shown at 2 sigma level and in some cases are smaller than the symbol size. Red symbols indicate outliers. The two open symbols at ~370 mm correspond to the two samples analyzed at the Isotope Laboratory, Xi'an Jiaotong University.

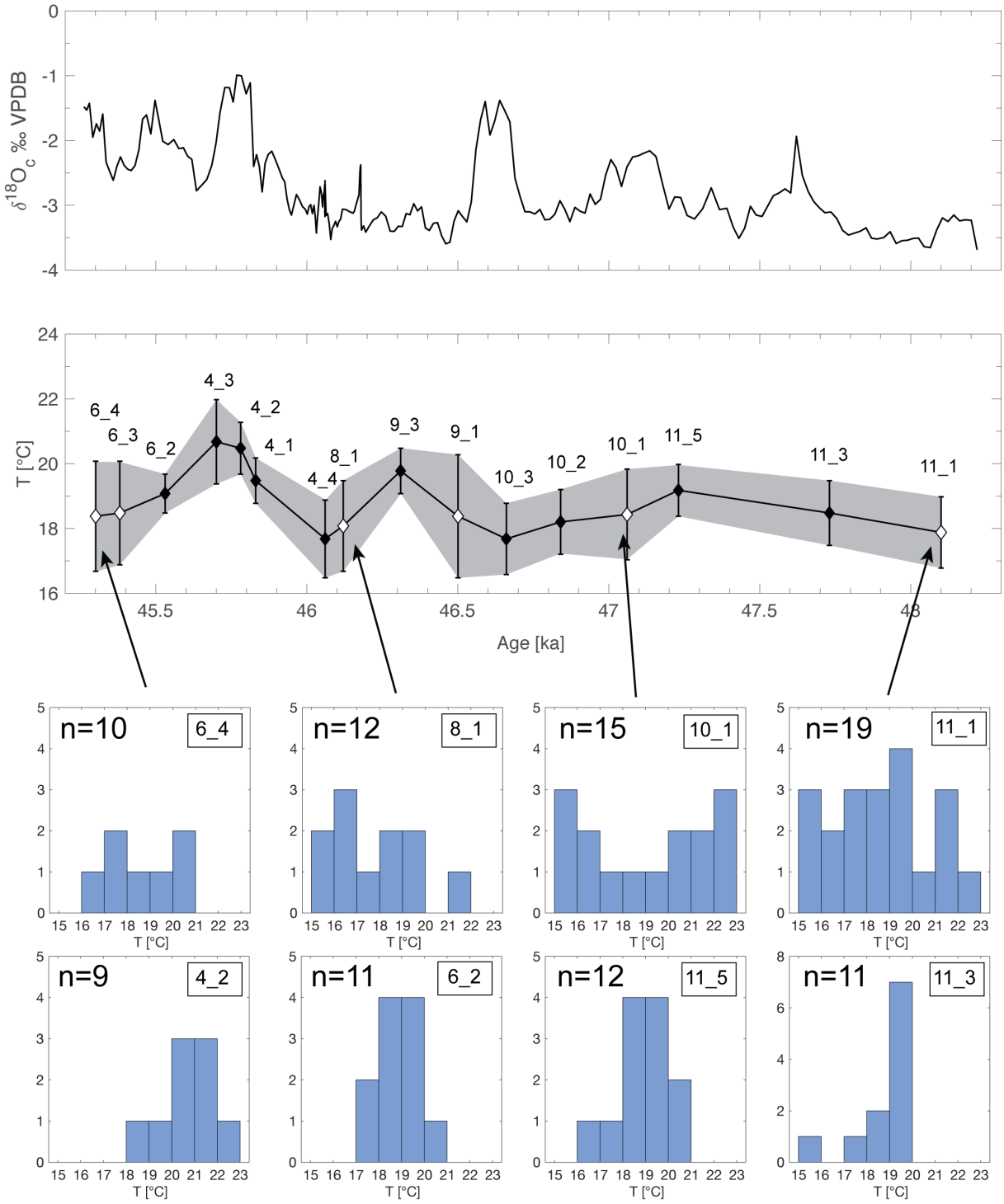

Figure S5:
Top. $\delta^{18}O_c$.
Middle. microthermometry temperatures with black symbols representing samples with a 3-6°C range and normal-like distribution and white symbols representing samples with larger ranges (6-9°C) and more uniform distributions.
Bottom. Examples of uniform distribution and large range of the replicate measurements (top row), and normal-like distribution with lower range of the replicate measurements (bottom row).

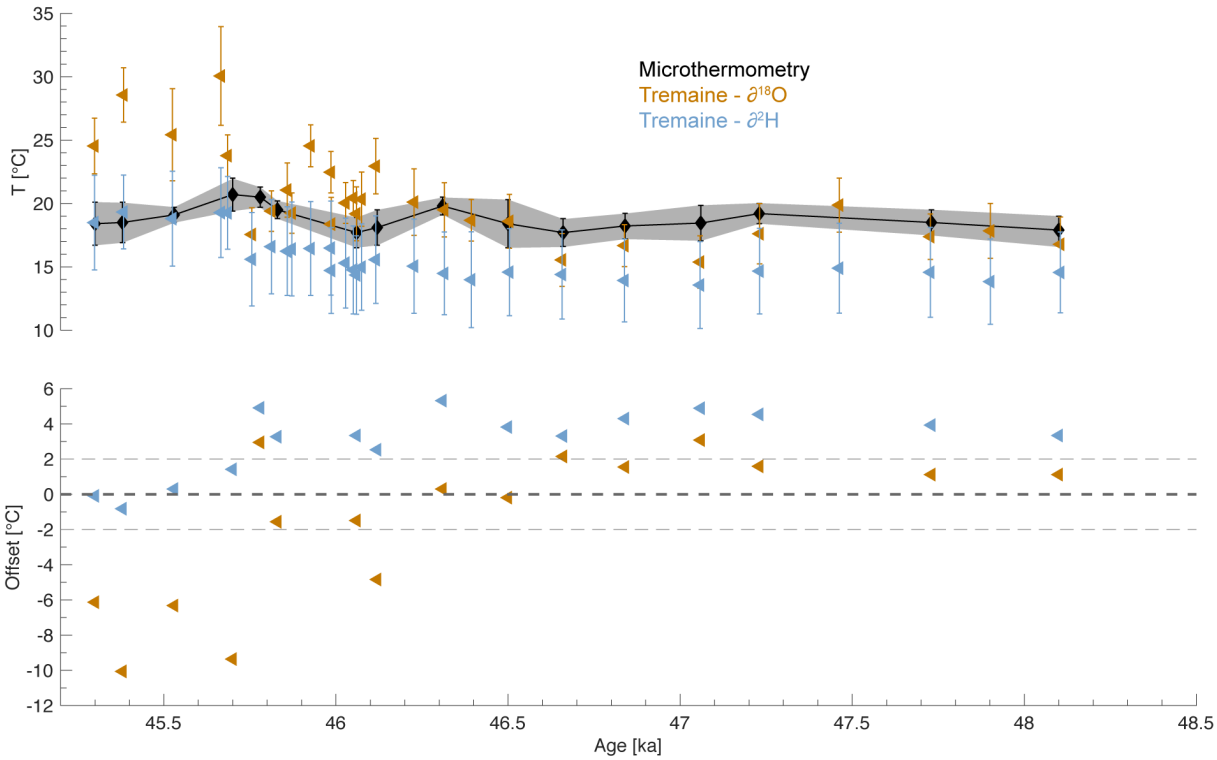

Figure S6: Top: comparison of temperature reconstructions from microthermometry (black diamonds) and FIWI (triangles) using the Tremaine et al. (2011) equation and measured $\delta^{18}O_c$ in combination with either the measured $\delta^{18}O_w$ (ochre) or $\delta^{18}O_w$ inferred from measured $\delta^{2}H_w$ and the local meteoric water line (light blue). The latter calculations give lower temperatures and larger error bars.
Bottom: temperature offset between microthermometry temperature and FIWI temperature calculated with either measured $\delta^{18}O_w$ (ochre) or $\delta^{18}O_w$ inferred from measured $\delta^{2}H_w$ and the local meteoric water line (light blue). Dashed lines indicate the 0 ± 2 °C range. Offsets are systematically higher with inferred $\delta^{18}O_w$ except for the four youngest samples where the estimations from the local meteoric water line show a better agreement with microthermometry.

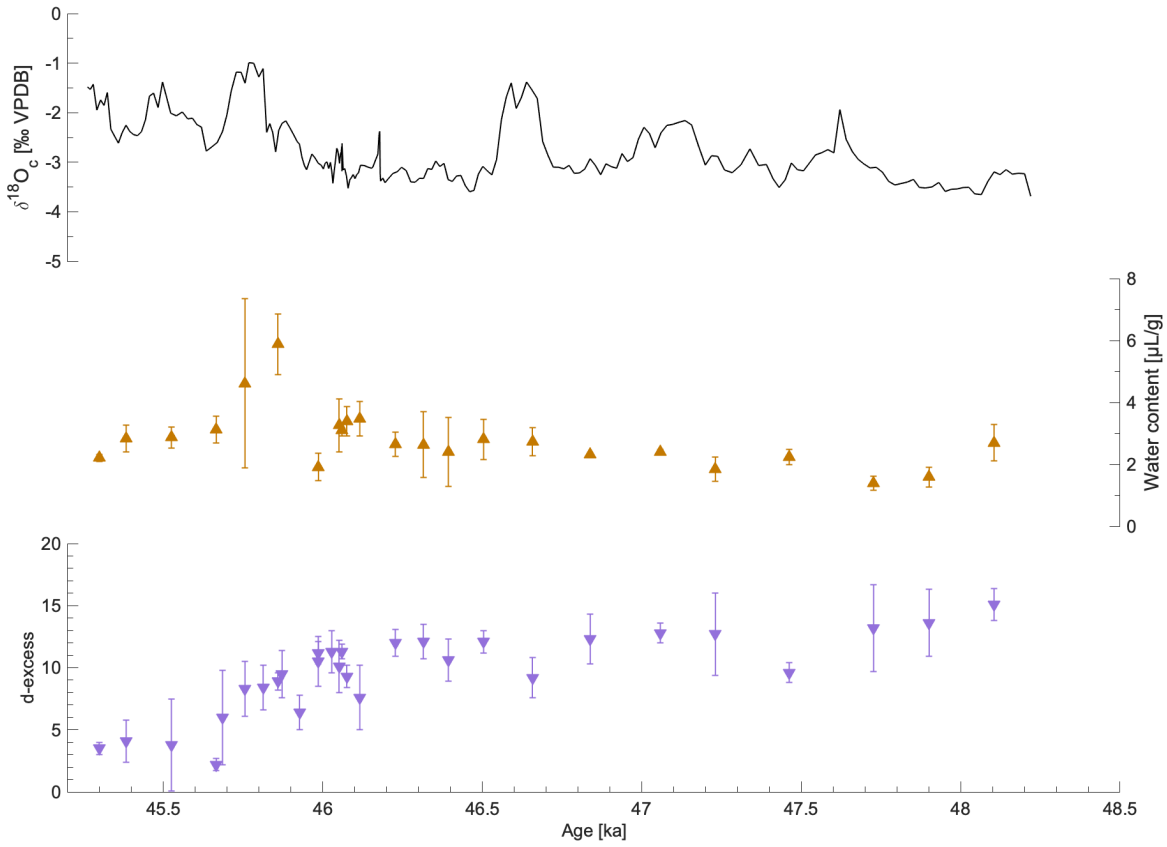

Figure S7: $\delta^{18}O_c$ (top), water content (middle) and d-excess (bottom). The water content is stable throughout the record except for a short increase ~45.8 ka. d-excess values are relatively constant from 48.3 to 46 ka and decrease to lower value from 46 to 45.2 ka.